Materials Chemistry and Physics 134 (2012) 747–754

Contents lists available at SciVerse ScienceDirect

Materials Chemistry and Physics

journal homepage: www.elsevier.com/locate/matchemphys

Excited nanoscale-TiO_2 induced interfacial electron transfer reaction of redox active cobalt(III)–alkyl amine complex and the solid surface

K. Anbalagan*, A.S. Ganeshraja, C. Maharaja Mahalakshmi

Department of Chemistry, Pondicherry University, Kalapet, Pondicherry 605 014, India

ARTICLE INFO

Article history:
Received 23 September 2011
Received in revised form
6 March 2012
Accepted 18 March 2012

Keywords:
Nano–TiO_2 photocatalysis
Interfacial electron transfer
Redox active complexes
Semiconductor photocatalysis
Photoreduction of adsorbate

ABSTRACT

Interfacial electron transfer reaction mechanism has been probed using $\lambda = 254$ nm excited TiO_2 nanoparticles and *cis*-$[Co^{III}(en)_2(RNH_2)Cl]Cl_2$ adsorbates (where RNH_2 = $MeNH_2$, $EtNH_2$, Pr^nNH_2, Bu^nNH_2, Bu^iNH_2, Pen^nNH_2, Hex^nNH_2, Bz^nNH_2) in aqueous 2-propanol. These tailor made complexes differing in coordination environment due to RNH_2 adhere onto TiO_2 surface producing compact nano-TiO_2// cobalt(III)–(RNH_2) surface compound. The surface of the anatase under UV irradiation is uniquely powerful as adsorbent due to inherent hydrophobic/hydrophilic properties. Therefore, the compact structure facilitates an efficient electron transfer to the Co(III) center resulting a high photoefficiency of formation of Co(II). A model for the electron transfer is arrived by considering: (i) the overlap of conduction band of TiO_2 with the acceptor level (Co center): (e^-, CB)/(e^-, tr) + (Co^{III}, ad) → Co^{II} and (ii) electronic coupling of donor level (localized on Ti center) with acceptor level (Co center): Ti (center) + (Co^{III}, ad) → Co^{II}. These pathways indicate accumulation of electron and appropriately available for reduction of the adhered complex ion. Significant insights were gained on the role of RNH_2 moiety in modifying compact structure of TiO_2–cobalt(III)–RNH_2 compound, redox power of semiconductor surface, and the proposed mechanism of interfacial electron transfer reactions.

1. Introduction

Titanium dioxide semiconductor has been widely investigated for promising applications in photoelectrochemical processes [1–3], dye-sensitized solar cells [4,5], and in photocatalytic reactions in response to growing environmental concerns [6,7]. The mechanism of photocatalytic reaction consists of photoinduced electronic processes such as, interfacial electron transfer (IFET)/ recombination of charges, catalyst surface-substrate affinity, donor/ acceptor characteristics and concentration, intensity and wavelength of excitation light, medium pH, redox potentials of substrates etc. Further, the fascinating structural, chemical and electronic properties of surface of metal oxides reveal crucial importance of solid surface in both catalytic and photocatalytic reactions. For instance, Stafford *et al.* observed [8] significant contributions of the direct electron transfer and surface chemical reactions in the ring cleavage reaction of 4-chloro phenol in TiO_2 suspensions. Similarly, a number of investigations were devoted to understand the feasible characteristics of both polycrystalline and nanocrystalline forms of titanium dioxide semiconductor particles in photocatalytic energy conversion schemes [4,5,9]. Nanostructures of materials represent a transition from crystal unit cells to bulk solid materials, which can exhibit novel reaction behaviors and physicochemical properties [10]. The high surface to volume ratio inherent in nanoparticles is useful for photocatalysis so most of the studies were focused on the nanosized particles with the purpose of improving the light absorption. Charge transfer processes at semiconductor–electrolyte interfaces are important toward fundamental understanding of the factors that control the kinetics and the development of alternatives to solid state photovoltaic devices for solar energy conversion [11]. An example of such a device is the dye-sensitized solar cell (Gratzel type cell), where a dye (transition metal complex) absorbs visible light and injects excited electron into the conduction band of a wide band gap semiconductor film, usually composed of nanoparticles [12]. The injected electron has been believed to enter into a conduction band state delocalized across the entire particle or in a state localized on an individual titanium center that is chemically bound with the substrate. The conduction band electron is then trapped in local sites within the particle. There is presently much effort directed toward characterizing and modeling interfacial charge transfer from molecular species to metals or semiconductors. The kinetics of

* Corresponding author. Tel.: +91 413 2654509; fax: +91 413 2655987.
E-mail address: kanuniv@gmail.com (K. Anbalagan).

0254-0584/$ – see front matter © 2012 Elsevier B.V. All rights reserved.
doi:10.1016/j.matchemphys.2012.03.063

both photoelectron injection and back reaction in dye-TiO_2 and other n-type metal oxide assemblies have been investigated, which reveal a complex not yet well understood series of processes.

The major aim of this investigation is to understand the redox activity of excited nano-TiO_2 and structurally modified cobalt(III) complexes, the latter is anticipated to interact with specific surface sites. Therefore, ancillary ligand (RNH_2) moiety was appended in *cis*-$[Co^{III}(en)_2(RNH_2)Cl]Cl_2$ complex, which was then coupled with the nano-TiO_2 to explore the possible role of structural and electronic features in IFET process. Ultimately, tailor made metal complexes can be employed in promoting photocatalytic activity and in photon harvesting by facile interfacial electron transfer.

2. Experimental

2.1. Materials and methods

$CoCl_2 \cdot 6H_2O$ (99%), alkyl amines (RNH_2), ferric chloride, potassium oxalate, sodium acetate, ammonium thiocyanate, nanocrystalline titanium dioxide, anatase, (surface area = 200–220 m^2g^{-1} and particle size = 25 nm) and DMSO-d_6 (NMR solvent) were purchased from Sigma Aldrich. 1,2-diamino ethane (LR), 1,10-phenanthroline and all other chemicals were purchased from Himedia and SD. Fine Chemicals (India). All the solvents and 1,2-diamino ethane were purified by distillation and water was triply distilled over alkaline $KMnO_4$ in an all glass apparatus. Analytically pure crystals of $[Co^{III}(en)_2(RNH_2)Cl]Cl_2$ (where RNH_2 = $MeNH_2$, $EtNH_2$, Pr^nNH_2, Bu^nNH_2, Bu^iNH_2, Pen^nNH_2, Hex^nNH_2, Bz^nNH_2) were synthesized by a modified procedure [13,14] and recrystallized.

2.2. Instrumentation

Cobalt(III) complexes were photolysed using 254 nm, 6 W low pressure mercury vapor lamp as light source (Germicidal G4T5, 3H, model 3006), in a small quartz immersion well (model 3210, 80 mL cap. Photochemical Reactors Ltd., UK). Electronic absorption spectral studies were undertaken on a double beam spectrophotometer (Shimadzu 2450, Japan) with integrating sphere attachment (ISR-2200). ^1H NMR measurements were made on a Bruker instrument; model Avance-II in 400 MHz Fourier transform–nuclear magnetic resonance with DMSO-d_6 solvent. Microscopic feature (AFM) of cobalt doped nano-TiO_2 at 300 K were collected on a Universal Scanning Probe Microscope (Innova SPM) in tapping mode imaging using silicon nitride cantilever probe with a nominal tip radius of 5–10 nm.

2.3. Photocatalytic activity measurement

The photocatalytic activity of nano-TiO_2 was evaluated by measuring the efficiency of reduction of $Co^{III}(en)_2(RNH_2)Cl^{2+}$ complex in neat water/aqueous 2-propanol solutions under 254 nm light irradiation. The photoefficiency was calculated by estimating photogenerated Co^{II} by Kitson's method [15]. Photoreduction was carried out in a reactor vessel using 254 nm low pressure mercury vapor lamp, which were housed in a fume hood (Lab Guard), covered with black polythene sheet to prevent extraneous light. The photoreactor is double walled quartz vessel, in which, photolyte mixture (100 mg of nano-TiO_2 crystals in 80 mL of $Co^{III}(en)_2(RNH_2)Cl^{2+}$ (1.98×10^{-3} M) solution and 1 M $NaNO_3$) was taken in the inner jacket and cool water in the outer jacket. Prior to irradiation, the suspension of the catalyst was achieved by ultrasonic treatment and continued to stir magnetically in dark to attain cobalt(III) complex ion adsorption/desorption equilibrium on the catalyst. The photolyte suspension was dosed with 254 nm light for definite irradiation periods (0, 2–16 min). About 4 mL aliquots were sampled and centrifuged to remove the semiconductor particles and then spectrally analysed. In order to diminish the experimental error, the experiments were repeated at least two-three times for the same sample and calculated the mean value. Photoefficiency of Co(II) formation in terms of percentage, PE (%) was computed using the formula: PE (%) = $[(A_t - A_i)/A_t]100$ where A_i and A_t are the absorbances of the photolysed solutions initially and at definite time interval 't' respectively.

3. Results and discussion

3.1. Photocatalytic reduction of adsorbate

Photoreduction of $Co^{III}(en)_2(RNH_2)Cl^{2+}$ was followed in presence/absence of nano-TiO_2 in order to benchmark the catalytic activity [16] (λ = 254 nm, water/2-propanol = 100/0-70/30 % (w/w). Cobalt(III)–RNH_2 complex is a good UV light absorber, however, decomposes on exposure to light over a long period of time [17–19] due to ligand to metal charge transfer (LMCT) bands (λ = ~226–230 nm and at ~362–366 nm). Surprisingly, addition of nano-TiO_2 (anatase) provoked the complex to degrade more efficiently and a higher amount of cobalt(II) was generated. The photocatalytic efficiency of anatase has been found to be efficient than rutile. Fig. 1 is a repetitive scan spectra of $Co^{III}(en)_2(MeNH_2)Cl^{2+}$ complex observed at definite irradiation time intervals; there is blue shift in the absorption maxima at $\lambda = 361 \rightarrow 349$ and $\lambda = 517 \rightarrow 499$ nm. Absence of isosbestic point in the repetitive scan spectra indicates the decomposition of the complex during reduction process suggesting perturbation of the Co^{III} center due to interfacial electron transfer. Fig. 2 illustrates a linear relationship of photoefficiency, PE (%) of formation of Co^{II} as a function of 2-propanol content. This implies the observed photoefficiency (Table 1) of formation of Co^{II} is a summation of the individual electron transfer reactions due to (i) excited nano-TiO_2: $Co^{III}(en)_2(RNH_2)Cl^{2+}$ + nano-TiO_2 + $h\nu$ (λ = 254 nm) → Co^{II} + products and (ii) ligand to metal charge transfer transition in cobalt(III) complex: $Co^{III}(en)_2(RNH_2)Cl^{2+} + h\nu$ (λ = 254 nm) → Co^{II} + products. However, the former path is predominant and requires a thorough investigation.

3.2. Probing of photoreduction by ^1H NMR

Photoproducts were identified by Kitson's [15] analytical method (Co^{II}) and ^1H NMR measurements (CH_3COCH_3). The

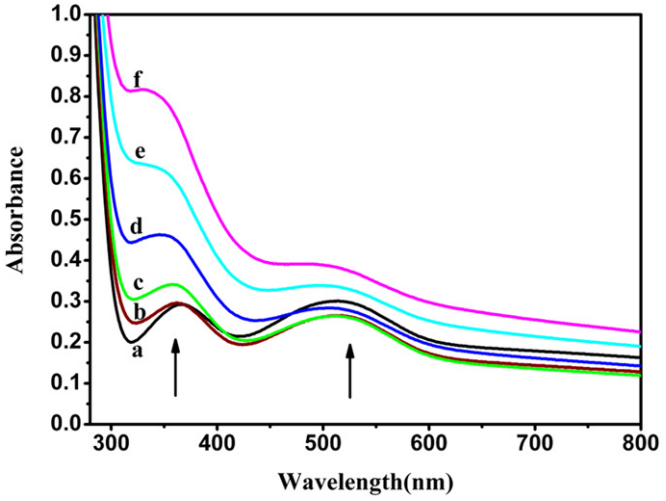

Fig. 1. Repetitive scan spectra recorded for the nano-TiO_2 photocatalysed reduction of $Co^{III}(en)_2(MeNH_2)Cl^{2+}$ complex in neat water and at various time intervals: (a) 0, (b) 2, (c) 4, (d) 8, (e) 12 and (f) 16 min respectively. Complex concentration = 1.98×10^{-3} M, ionic strength = 1 M $NaNO_3$, pH = 7.5, at 300 K.

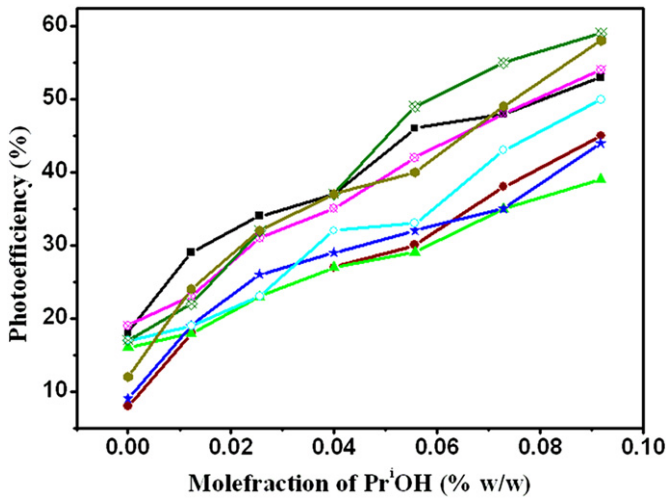

Fig. 2. Linear relationship between photoefficiency of Co(II) formation *vs.* x (Pr^iOH) in the reduction of $Co^{III}(en)_2(RNH_2)Cl^{2+}$ by excited nano-TiO_2. $Co^{III}(en)_2(RNH_2)Cl^{2+}$ complexes: RNH_2 = $MeNH_2$, $EtNH_2$, $PrNH_2$, $BuNH_2$, Iso-$BuNH_2$, $PentNH_2$, $HexNH_2$ and $BzNH_2$.

photoreduction was systematically followed by NMR measurements which indicate the growth of acetone peak progressively appearing in signal intensity as a function of dosage of light. Fig. 3 exhibits ^1H NMR signals due to 2-propanol appearing at $\delta = 1.0–1.1$ ppm ($-CH_3$) and $\delta = 3.71–3.83$ ppm ($-CH$) before the initiation of photoreduction and after definite time of irradiation periods. There is a steady growth of signal due to photoreleased acetone and the signal intensity increases with respect to dosage of light. That is, new ^1H NMR signal at $\delta = 2.04$ ppm indicates the formation of acetone and the signal strength (Table 2) has increased considerably with increase in time of irradiation [20]. In fact, the integrated intensity of the acetone signals gradually increase, whereas the $-CH$ and $-CH_3$ (2-propanol) signals gradually decrease. These results are in close agreement with that of an earlier study [21] on the decomposition of 2-propanol, in which UV irradiation induced decomposition of gaseous 2-propanol by TiO_2 thin film released an equal amount of acetone as a product. The origination of acetone is from the oxidation of 2-propanol resulting due to scavenging [22] of the valence band holes by alcohol: nano-TiO_2 (h^+) + $(CH_3)_2CHOH \rightarrow CH_3COCH_3$. This kind of hole scavenging enhanced electron carrier density available for reduction of Co(III) center and retarded e^-/h^+ pair recombination probability.

3.3. Mechanism of interfacial electron transfer

It is apparent from Table 1 that excited nano-TiO_2 shows better catalytic activity, which critically depends upon surface–substrate interaction. Surface affinity of molecules/ions is a competing feature of surface [23], therefore, formation of nano-TiO_2// cobalt(III)–(RNH_2) surface compound is inevitable. Therefore, an enhancement in photocatalytic reduction originates from (i) surface–substrate interaction; it means the $-CH_2/-CH$ units of the sixth ligand, RNH_2 can modify surface affinity of $Co^{III}(en)_2(RNH_2)Cl^{2+}$ ion with the nano-TiO_2 surface and (ii) photoexcitation can prompt the formation of microdomains in nano-TiO_2 with characteristic hydrophobic/hydrophilic behavior. Thereby accumulation of adsorbate is varied and hence available for reduction. In addition, charge relaxation/recombination processes of nano-TiO_2 (e^-, h^+) pair are altered due to the formation of compact nano-TiO_2// cobalt(III)-(RNH_2) surface compound, (Co^{III}_{ad}). Such processes provide a favorable negative charge potential for reduction of Co(III) center. Thus, the overall efficiency of heterogeneous photocatalysis is determined by the adsorbate content and population/ lifetime of charge carriers for interfacial charge transfer processes [24,25]. Sixth ligand (RNH_2) in $Co^{III}(en)_2(RNH_2)Cl^{2+}$ with hydrophobic tail imparts variation in surface adherence of the complex ion on the surface of nano-TiO_2, however the adsorption process is restricted by thermodynamic aspects. To rationalize these observations, one must invoke a mechanism that incorporates several complementation routes as given in eqs. (1–7).

Surface compound formation: nano-TiO_2 + $Co^{III}(en)_2(RNH_2)Cl^{2+}$ → nano-TiO_2//$Co^{III}(en)_2(RNH_2)Cl^{2+}$ (1)

Photoexcitation: nano-$TiO_2 + h\nu \rightarrow$ nano-TiO_2 (e^-, CB) + nano-TiO_2 (h^+, VB) (2)

Charge trapping: (e^-, CB) → (e^-, tr) (3)

(h^+, VB) → (h^+, tr) (4)

Table 1
Photoefficiency P.E (%) of formation of Co(II) upon $\lambda = 254$ nm irradiation of *cis*-$[Co^{III}(en)_2(RNH_2)Cl]Cl_2$ in aqueous 2-propanol at 300 K. Photocatalyst nano-TiO_2, ionic strength 1 M $NaNO_3$, complex concentration = 1.98×10^{-3} M.

RNH_2 in alkyl amine	PE(%) in water/Pr^iOH (w/w)								Slope value × 10^2	pKa value of RNH_2 in alkyl amine
		100/0	95/5	90/10	85/15	80/20	75/25	70/30		
$MeNH_2$	–	13	18	27	28	30	32	34	2.85	10.64
	nano-TiO_2	18	29	34	37	46	48	53	3.05	
$EtNH_2$	–	7	15	20	24	27	30	31	3.75	10.67
	nano-TiO_2	8	18	23	27	30	38	45	3.94	
Pr^nNH_2	–	5	12	15	16	23	28	29	3.00	10.53
	nano-TiO_2	16	18	23	27	29	35	39	3.23	
Bu^nNH_2	–	7	17	23	24	26	27	33	3.05	10.56
	nano-TiO_2	9	19	26	29	32	35	44	3.33	
Bu^iNH_2	–	9	16	17	20	22	27	35	2.85	10.59
	nano-TiO_2	17	19	23	32	33	43	50	3.61	
Pen^nNH_2	–	6	9	19	23	24	29	37	3.18	10.63
	nano-TiO_2	19	23	31	35	42	48	54	4.00	
Hex^nNH_2	–	8	14	17	24	25	28	32	3.09	10.56
	nano-TiO_2	17	22	32	37	49	55	59	5.33	
$BzNH_2$	–	5	17	25	26	29	30	31	3.51	9.38
	nano-TiO_2	12	24	32	37	40	49	58	5.00	

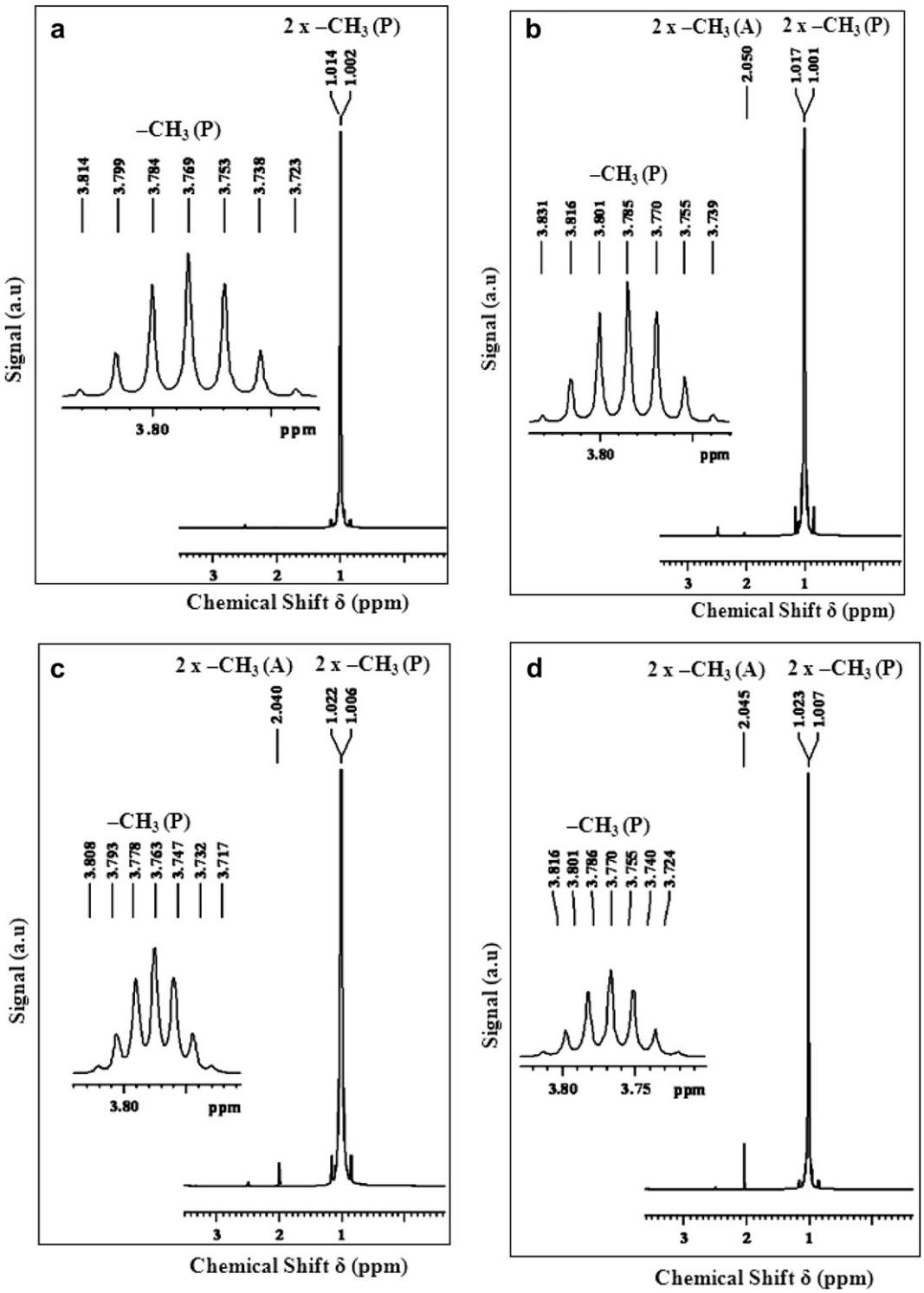

Fig. 3. ^{1}H NMR spectra (in DMSO-d_6) profile from the photocatalysed nano-TiO_2/$Co^{III}(en)_2(MeNH_2)Cl^{2+}$ decomposition of 2-propanol at various time intervals: (a) 0, (b) 8, (c) 16 and (d) 45 min respectively. 'A' and 'P', respectively, denote acetone and 2-propanol. The inset shows the −CH signal of 2-propanol appearing in the region 3.71–3.83 ppm, complex concentration = 1.98×10^{-3} M, ionic strength = 1 M $NaNO_3$, pH = 7.5 and at 300 K.

Electron-hole recombination: $(e^-, tr)/(e^-, CB) + (h^+, tr)/(h^+, VB) \rightarrow (e^-, tr) + heat$ (5)

Electron transfer: $\text{nano}-TiO_2(e^-, CB)/\text{nano}-TiO_2(e^-, tr) + \left(Co^{III}_{ad}\right) \rightarrow Co^{II}_{surf} + Co^{II}_{aq}$ (6)

Hole transfer: nano-TiO_2 (h^+, VB)/nano-TiO_2 $(h^+, tr) + (CH_3)_2CHOH \rightarrow CH_3COCH_3$ (7)

Where (e^-, tr) and (h^+, tr) represent charge trapped surface states while Co^{III}_{ad}, Co^{II}_{surf}, and Co^{II}_{aq} represent surface compound, surface implanted species and aqueous species respectively. It is unlikely that the photoreduction of Co(III) proceeds through

Table 2
^{1}H NMR data for the generation of acetone upon $\lambda = 254$ nm irradiation of *cis*-$[Co^{III}(en)_2(MeNH_2)Cl]Cl_2$ at 300 K. Photocatalyst nano-TiO_2, ionic strength 1 M $NaNO_3$, complex 1.98×10^{-3} M 'A' and 'P', respectively, denote acetone and 2-propanol, NMR solvent is DMSO-d_6.

Irradiating time (min)	2× $-CH_3$(d)$P\delta$ ppm		$-CH$(m)$P\delta$ ppm							2× $-CH_3$(s) $A\delta$ ppm
0	1.014	1.002	3.723	3.738	3.753	3.769	3.784	3.799	3.814	–
8	1.001	1.017	3.739	3.755	3.770	3.785	3.801	3.816	3.831	2.050
16	1.006	1.022	3.717	3.732	3.747	3.763	3.778	3.793	3.808	2.040
45	1.007	1.023	3.724	3.740	3.755	3.770	3.786	3.801	3.816	2.045

multielectron process, but it should occur in one electron step. The predominant reduction path of the metal center is as given in eq. (6) with a limited contribution from charge transfer population states like: $\sigma(N) \rightarrow d\sigma^*(Co)$ and $\sigma(Cl) \rightarrow Co$.

3.4. Optimized structure of adsorbate ion

Titanium dioxide semiconductor is not susceptible to redox or passivation processes that are prevalent in small-band gap semiconductors. Therefore, the surface-adsorbed ion is the target in photoredox reaction due to interfacial electron transfer (IFET) between semiconductor particle and the adhered species. Generally, metal complexes do show surface affinity, for instance, Langmuir adsorption isotherm on porphyrin [26] binding onto TiO_2 in toluene and surface attachment of phthalocyanine dyes [27] onto nanocrystalline TiO_2 were reported in earlier studies. It is interesting to note that the PE (%) of Co^{II} generation is (i) linearly increasing with 2-propanol content and (ii) showing some relationship with variation in the RNH_2 ligand of the complex and this non-consistency can be attributed due to nanoparticle surface// cobalt(III)–RNH_2 affinity and subsequent interfacial electron transfer. Accumulation of cobalt(III) complex onto the surface of anatase to form a compact layer is mainly depending upon the blocking effect of RNH_2 due to hydrophobic and steric hindrance. Pellizzetti and co-workers [28] showed a significant alteration in the distribution of aromatic intermediates on the surface of TiO_2 in an earlier study. Scheme 1 represents achieving of the photoinduced interfacial electron transfer at the surface of the semiconductor due to: (i) surface adsorption of the species $Co^{III}(en)_2(RNH_2)Cl^{2+}$ influenced by the hydrophobic and steric effects of RNH_2 moiety due to the $-CH_2/-CH$ units and (ii) hole scavenger such as 2-propanol.

Fig. 4 illustrates photoefficiency data for the complexes plotted against the number of carbon atoms of $-CH_2/-CH$ units in RNH_2 group as a measure of hydrophobic contribution of the complex ion. The fact that PE varies by *ca.* 10–27% over this collection of complexes indicating some influence must shift the Fermi energy level of TiO_2. This effect is ascribed to a shift in the conduction band edge of TiO_2 upon adsorption of the complex ion and the magnitude of this shift is related to the nature of the coordination sphere. Gratzel *et al.*, reported [29] the transient absorbance decay kinetics of oxidized *cis*-$Ru(dcbpy)_2(NCS)_2$ in presence of $Co(dbbip)_2^{2+/3+}$ mediator due to adsorption on TiO_2 semiconductor surface. The ultrafast injection of electrons from nano-TiO_2 (e^-, h^+) to cobalt(III) complex is due to surface attachment of the complex ion. In general, the nanoparticles have many active sites [30,31] for adsorption of molecular donors/acceptors so that the probability of interfacial electron transfer is well organized relative to that of bulk material. The hydrophobic/hydrophilic microdomain structures of excited nano-TiO_2 inevitably improves the surface accumulation of $Co^{III}(en)_2(RNH_2)Cl^{2+}$ by altering the binding force. A systematic variation of ancillary ligand, in this case, amino alkane may help to indicate the importance of electronic delocalization in electron transfer reactions. Qualitatively, the electron trapping and electron-hole relaxation/recombination bring the question of role of solvent/solvent [32] mixtures. Therefore, suitably modified coordination structure can compete with electron-hole relaxation/recombination process due to variation in surface affinity.

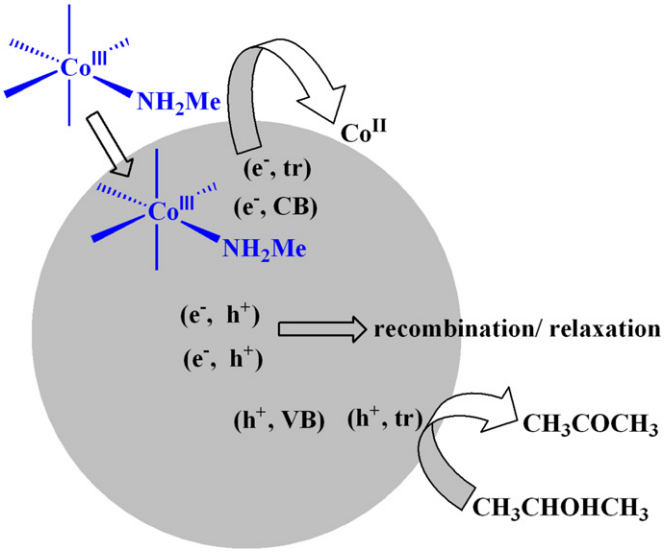

Scheme 1. Photoreduction mechanism of $Co^{III}(en)_2(RNH_2)Cl^{2+}$complex as surface-adsorbed species on nano-TiO_2 particle in water/2-propanol mixture at 300 K.

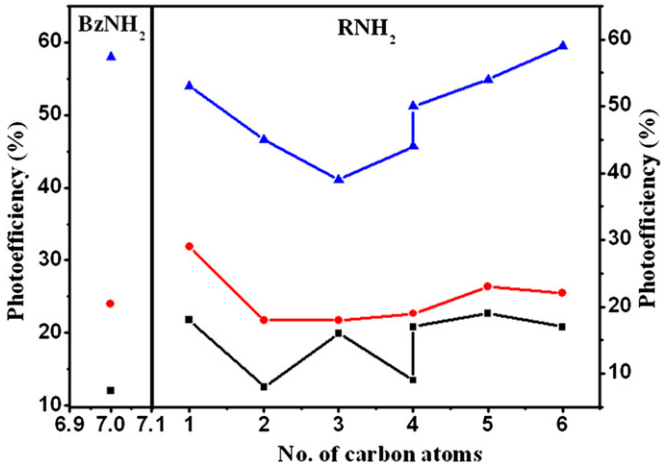

Fig. 4. Linear relationship between photoefficiency obtained for $Co^{III}(en)_2(RNH_2)Cl^{2+}$/nano-$TiO_2$ *vs.* no. of carbon atoms in alkyl amine (RNH_2) in $Co^{III}(en)_2(RNH_2)Cl^{2+}$ with the presence of nano-TiO_2 in ▬■▬ neat water, ▬●▬ 95/5 (w/w)% water/Pr^{i}OH, ▬▲▬ 70/30 (w/w)% water/Pr^{i}OH.

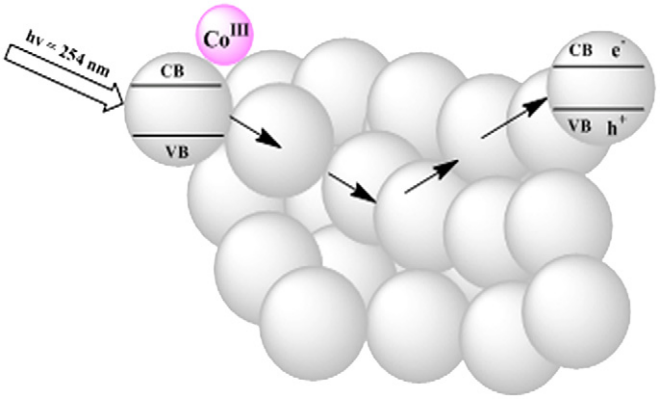

Scheme 2. Electronic coupling between adhered complex ion and the conduction band states of anatase is stronger than coupling between states spread over particles.

3.5. Site isolated surface species reduction

The photoefficiency of Co^{II} formation is mainly influenced by two factors: surface-complex ion interaction leading to the formation of compact surface site//cobalt(III)–RNH_2 compound [33,34] and charge transfer/recombination. First one is interesting and requires some understanding while the second is due to solvent environment. The electronic coupling between adhered complex ion and the conduction band states of the semiconductor particles is stronger than electronic coupling between states that have their density spread throughout the nanoparticle system (Scheme 2). The density of states for the conduction band is expected to rise proportionately to the $\varepsilon^{1/2}$, where ε is the energy above the conduction band edge [35]. Electronic structure calculations of anatase show density of states rises sharply from 0.5 to 2 eV above the edge [36,37]. Hence, conduction band electrons are presumed to be distributed into states well above the conduction band edge, nano-TiO_2 (e^-, CB) as well as in surface trap states, nano-TiO_2 (e^-, tr). Therefore, more effective electron transfer pathways can be generated via this compact nano-TiO_2//cobalt(III)–(RNH_2) compound. That is, close proximity in TiO_2//Co^{III} compound can influence electron transfer into the acceptor orbital of the complex from excited nano-TiO_2. The prerequisite is the well defined and uniform adherence of the complex ion on the surface of the excited nano-TiO_2. Such arrangement is determined by the coordination environment of the Co(III) center, more precisely the alkyl chain of the (RNH_2) ligand significantly contributes in the adherence due to bulkiness, polarity etc. That is molecular orientation of the adsorbate becomes ordered/disordered such spatial freedom alters the electronic coupling between the complex ion and the conduction band states. Therefore, the ligand acts as anchoring group thereby the complex ion binds to the surface either weakly/strongly to the solid substrate, for instance, a recent study illustrated that molecular arrangement was found to contribute significantly in the interfacial electron transfer [38,39] process. Ultimately, a model may be arrived which assumes the charge transfer is due to (i) conduction band into acceptor level (Co center): $(e^-, CB)/(e^-, tr) + (Co^{III}_{ad}) \rightarrow Co^{II}_{surf} + Co^{II}_{aq}$ and (ii) electronic coupling of donor level (localized on Ti center) with acceptor level (Co center): $Ti(center) + (Co^{III}_{ad}) \rightarrow Co^{II}_{surf} + Co^{II}_{aq}$. The electronic coupling between cobalt(III)–RNH_2 center and the conduction band states is expected to be dependent of energy. States

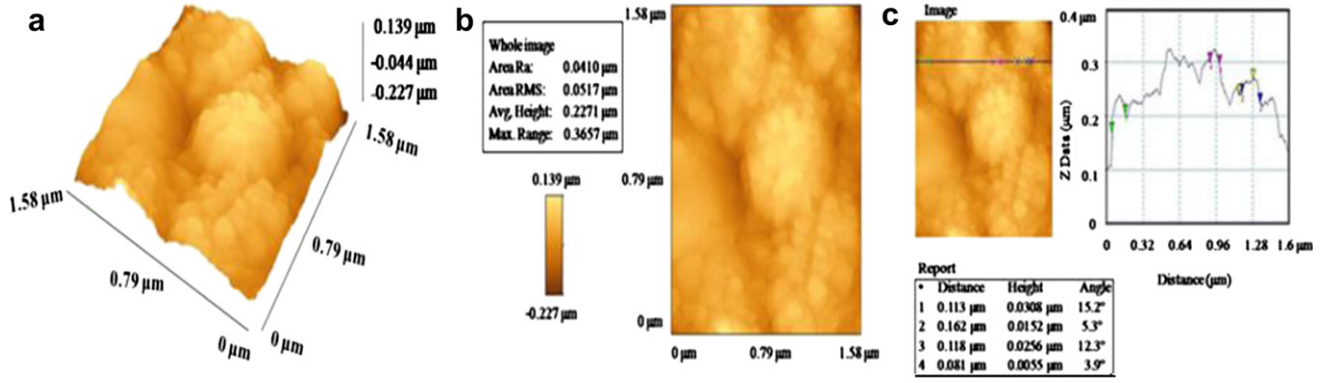

Fig. 5. Atomic force microscopic images of the catalyst, nano-TiO_2, obtained at 0 s (before the light is doused).

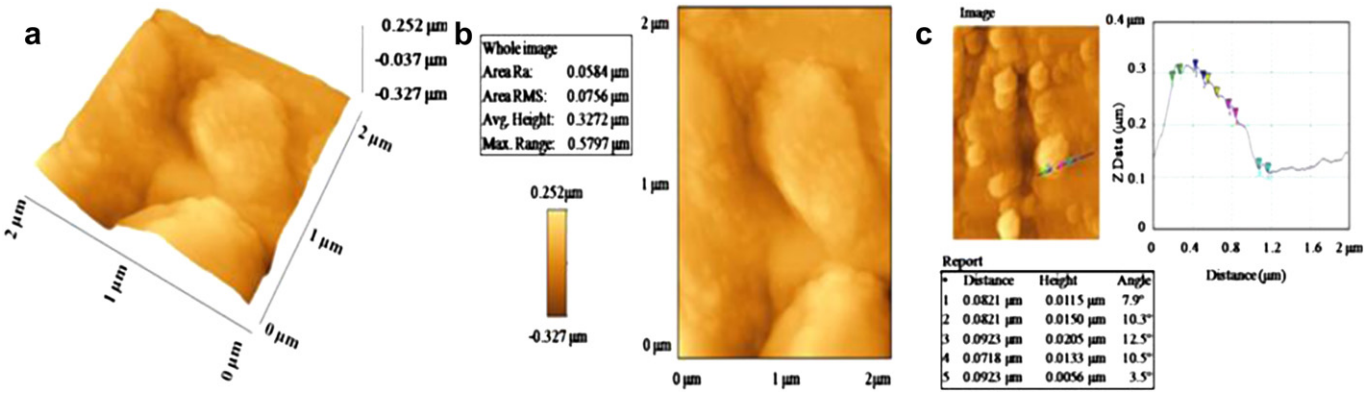

Fig. 6. Atomic force microscopic images of nano-TiO_2 catalyst collected after 120 s dosage of light.

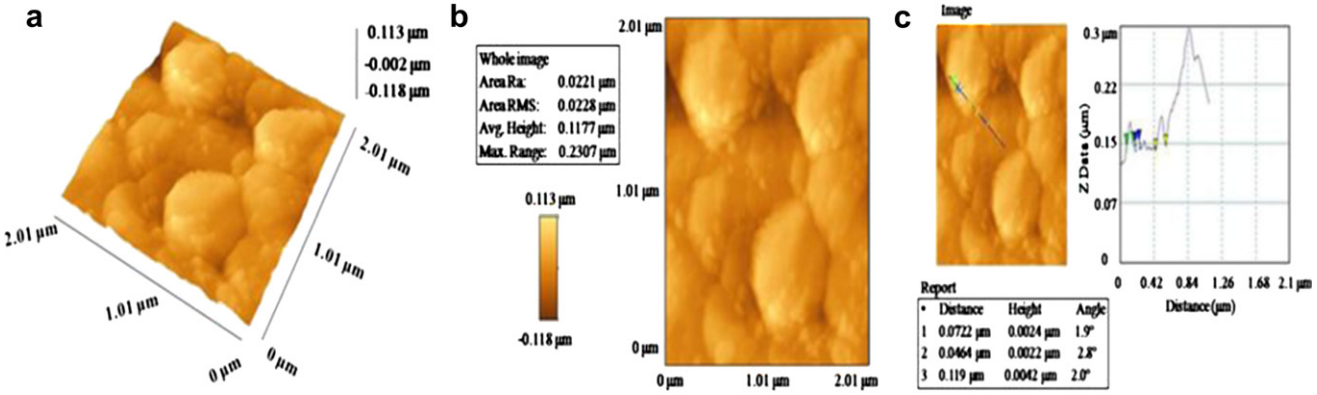

Fig. 7. Atomic force microscopic images of nano-TiO_2 catalyst collected after 720 s dosage of light.

that have a significant portion of their electron density on Ti center with which cobalt(III)–(RNH_2) is bound would be more strongly coupled to the Co center [40,41]. The compact surface site//cobalt(III)–RNH_2 compound formation enables electron injection into Co-*d* orbital from (i) orbital primarily residing on Ti center that is close to the point of attachment of cobalt(III) complex and (ii) delocalized conduction band states. It is more probable that pathway (i) contributes predominantly than that of (ii) route. Therefore, the interfacial electron transfer depends upon (i) structure and geometry of cobalt(III) complex, (ii) conduction band/electronic coupling of donor level with acceptor level and (iii) relaxation/recombination processes.

3.6. Surface morphology of catalyst

Typical morphologies of the catalyst, nano-TiO_2, isolated before (Fig. 5; 0 s) and after definite time of irradiation periods (Fig. 6; 120 s and Fig. 7; 720 s) were investigated using AFM images. The AFM images presented in Figs. 6 and 7 consist of grains with similar shape, but with remarkably reduced grain size. The atomic force microscopy (AFM) measurements show relevant changes in surface topography in the probed areas $1.58 \times 1.58\ \mu m^2$ and $2 \times 2\ \mu m^2$. The AFM images shown in Figs. 5–7 composed [42] of uniformly distributed grains with average height: ~0.327 μm–~0.118 μm and the distance of ~0.131 μm to ~0.076 μm. Surface morphology was characterized by the 3D images, which show particles packed surface rather than sheet-packed [43,44] surface. The 3D images obviously illustrate (Figs. 5–7a) the variation in the surface morphology, which seems to be composed of compact islands. Each TiO_2 particle has nearly spherical shape and consists of many nanocrystallites, however some particles are combined into larger agglomerates and form structures up to 0.04 μm (Fig. 5a). The surfaces are rougher than pure nano-TiO_2 and the additional roughness in irradiated nano-TiO_2 is due to surface topographical features, which imply the existence of defect or coordination sites. The features of grains measured at various angles indicate near equidistance and relatively smooth, similarly, the grains align along a line at one direction show resemblance in properties. The height variation parameters closely resemble in the ultrafine samples and observed to be well defined with characteristic grain boundaries. The AFM images show that surface roughness closely resemble (0.0756–0.0288 μm RMS), obviously, the surface coverage is crystalline and implies potential for chemical implantation. An enhancement in rms roughness is a measure of the extension [45–47] of micorfacets, which are types of defects. Therefore, change in grain shape must be regulated from a change of the relative surface energies due to the existence of impurity particles at the grain boundaries. That is, a considerable change indicates the surface of nano-TiO_2 is modified due to the interaction [10] of the complex ion as adsorbate and the product Co^{II} ion. The size of nanoparticle from AFM images was extremely different from the XRD calculated ones [10] (~11 nm) due to the tendency of nanoparticles to form agglomerates [48] in local region. The features of grains measured at various angles illustrate the smoothness and property resemblance. The crystalline quality becomes smooth at higher dosage of light, which enhanced the Co(III)/Co(II) density on the surface. This indicates a facile surface compound formation, surface site//cobalt(III)–RNH_2, the latter is dictated by the alkyl ligand and hence the photoreduction of the adsorbate complex ion.

4. Conclusion

Photocatalytic efficiency of nanoparticle anatase is a function of the adsorbates ability to promote interfacial electron transfer and inhibit relaxation/recombination of electron-hole pair. Cobalt(III) complexes with alternate structure consisting of RNH_2 can become suitable redox active agents, which have varied surface affinity due to the hydrophobic/steric effects of the alkyl amine ligand. The photocatalytic activity can be explained by the (i) applicability of tailor made cobalt(III) complexes, (ii) efficiency of formation of compact nano-TiO_2/cobalt(III)–(RNH_2) compound using microdomains formed with characteristic hydrophobic/hydrophilic abilities and (iii) alternative structure (TiO_2/Co^{III}) which provides facilitative mechanism for directional movement of electrons into Co-*d* orbital from states above the conduction band edge (e^-, CB), surface trap states (e^-, tr) and localized states of Ti center. AFM measurements indicate a high crystalinity of the catalyst and the possible formation of surface compound as the irradiation time proceeds. The investigation on the electron transfer from TiO_2 (h^+, e^-) into Co^{III} answers many questions about the primary steps in the photoinduced redox processes. The major findings are; (i) electron holding ability on excited TiO_2 can be systematically probed and (ii) a species adsorbed onto the nano-TiO_2, the electron transfer reaction can successfully compete with the relaxation/recombination of electron-hole taking place in picosecond time scale.

Acknowledgment

KA records his sincere thanks to the Council of Scientific and Industrial Research-HRDG, New Delhi, for financial support through major research project. The authors thank CIF, Pondicherry University and Veeco-India Nanotechnology Laboratory, JNCASR, Bangalore for providing instrumental facility.

References

[1] N. Fu, Y. Wu, Z. Jin, G. Lu, Langmuir 26 (2010) 447–455.
[2] A. Fujishima, K. Honda, Nature 238 (1972) 37–38.
[3] M. Gratzel, Nature 414 (2001) 338–344.
[4] (a) J.S. Im, S.K. Lee, Y.S. Lee, Appl. Surf. Sci. 257 (2011) 2164–2169;
(b) B. Oregan, M. Gratzel, Nature 353 (1991) 737–740.
[5] A.B.F. Martinson, T.W. Hamann, M.J. Pellin, J.T. Hupp, Chem. Eur. J. 14 (2008) 4458–4467.
[6] T.L. Thompson, J.T. Yates, Chem. Rev. 106 (2006) 4428–4453.
[7] (a) Y.C. Tang, X.H. Huang, H.Q. Yu, L.H. Tang, Int. J. Photoenergy (2012) doi: 10.1155/2012/960726;
(b) X. Chen, S.S. Mao, Chem. Rev. 107 (2007) 2891–2959.
[8] U. Stafford, K.A. Gray, P.V. Kamat, J. Catal. 167 (1997) 25–32.
[9] A. Fujishima, T.N. Rao, D.A. Tryk, J. Photochem. Photobiol. C 1 (2000) 1–21.
[10] K. Anbalagan, J. Phys. Chem. C 115 (2011) 3821–3832.
[11] T.W. Hamann, F. Gstrein, B.S. Brunschwig, N.S. Lewis, Chem. Phys. 326 (2006) 15–23.
[12] J.A. Harris, K. Trotter, B.S. Brunschwig, J. Phys. Chem. B 111 (2007) 6695–6702.
[13] K. Anbalagan, M. Tamilselvan, S. Nirmala, L. Sudha, Acta Crystallogr. Sect. E: Struct. Rep. Online E65 (2009) m836–m837.
[14] K. Ravichandran, P. Ramesh, M. Tamilselvan, K. Anbalagan, M.N. Ponnuswamy, Acta Crystallogr. Sect. E: Struct. Rep. Online E65 (2009) m1174–m1175.
[15] R.E. Kitson, Anal. Chem. 22 (1950) 664–667.
[16] P. Paopresert, J.E. Laaser, W. Xiong, R.A. Franking, R.J. Hamers, M.T. Zanni, J.R. Schimidt, P. Gopalan, J. Phys. Chem. C 114 (2010) 9898–9907.
[17] K. Anbalagan, T. Geethalakshmi, S.P.R. Poonkodi, J. Phys. Chem. A 107 (2003) 1918–1927.
[18] K. Anbalagan, A. Rajendran, J. Photochem. Photobiol. A 182 (2006) 128–136.
[19] K. Anbalagan, I.S. Lydia, Spectrochim. Acta A 69 (2008) 964–970.
[20] S. Matsuo, N. Sakaguchi, K. Yamada, T. Matsuo, H. Wakita, Appl. Surf. Sci. 228 (2004) 233–244.
[21] Y. Ohko, K. Hashimoto, A. Fujishima, J. Phys. Chem. A 101 (1997) 8057–8062.
[22] S. Ardo, G.J. Meyer, J. Am. Chem. Soc. 132 (2010) 9283–9285.
[23] K. Anbalagan, C. Maharaja Mahalakshmi, A.S Ganeshraja, J. Mol. Struct. 1005 (2011) 45–52.
[24] C. Creutz, B.S. Brunschwig, N. Sutin, J. Phys. Chem. B 110 (2006) 25181–25190.
[25] S. Ardo, Y. Sun, A. Staniszewski, F.N. Castellano, G.J. Meyer, J. Am. Chem. Soc. 132 (2010) 6696–6709.
[26] D.F. Watson, A. Marton, A.M. Stux, G.J. Meyer, J. Phys. Chem. B 107 (2003) 10971–10973.
[27] A. Zaban, S. Ferrere, B.A. Gregg, J. Phys. Chem. B 102 (1998) 452–460.
[28] C. Minero, G. Mariella, V. Maurino, E. Pellizzetti, Langmuir 16 (2000) 2632–2641.
[29] V. Shklover, M.K. Nazeeruddin, S.M. Zakeeruddin, C. Barbe, A. Kay, T. Haibach, W. Steurer, R. Hermann, H.U. Nissen, M. Gratzel, Chem. Mater. 9 (1997) 430–439.
[30] K. Anbalagan, L. Devaraj Stephen, Transition Met. Chem. 34 (2009) 915–923.
[31] H. Nusbaumer, J.E. Moser, S.M. Zakeeruddin, M.K. Nazeeruddin, M. Gratzel, J. Phys. Chem. B 105 (2001) 10461–10464.
[32] K. Anbalagan, I.S. Lydia, J. Phys. Org. Chem. 24 (2011) 45–53.
[33] J.C. Yu, J. Yu, H.Y. Tang, L. Zhang, J. Mater. Chem. 12 (2002) 81–85.
[34] S.K. Weit, P.A. Grutsch, C. Kutal, Inorg. Chem. 30 (1991) 2819–2821.
[35] S.M. Sze, Semiconductor devices, Physics and Technology, second ed. Wiley, New York, 2002.
[36] Q. Chen, H.H. Cao, Chin. Phys. 13 (2004) 2121–2125.
[37] R. Asahi, Y. Taga, W. Mannstadt, A.J. Freeman, Phys. Rev. B 61 (2000) 7459–7465.
[38] H. Imahori, H. Norieda, H. Yamada, Y. Nishimura, I. Yamazaki, Y. Sakata, S. Fukuzumi, J. Am. Chem. Soc. 123 (2001) 100–110.
[39] H. Imahori, H. Yamada, Y. Nishimura, I. Yamazaki, Y. Sakata, J. Phys. Chem. B 104 (2000) 2099–2108.
[40] T. Sakata, K. Hashimoto, M. Hiramotoff, J. Phys. Chem 94 (1990) 3040–3045.
[41] K.A. Walters, D.A. Gaal, J.T. Hupp, J. Phys. Chem. B 106 (2002) 5139–5142.
[42] A.N. Okte, E. Sayinsoz, Sep. Purif. Technol. 62 (2008) 535–543.
[43] T. Bezrodna, G. Puchkovska, V. Shymanovska, A. Hauser, J. Phys. Chem. Solids 66 (2005) 1057–1063.
[44] T.C. Kaspar, T. Droubay, D.E. McCready, P. Nachimuthu, S.M. Heald, C.M. Wang, A.S. Lea, V. Shutthanandan, S.A. Chambers, M.F. Toney, J. Vac. Sci. Technol. B 24 (2006) 2012–2017.
[45] C.M. Teodorescu, G. Socol, C. Negrila, D. Luca, D. Macovei, J. Exp. Nanosci. 5 (2010) 509–526.
[46] J. Li, C.H. Sow, X.S. Rao, C.K. Ong, D.N. Zheng, Eur. Phys. J. B 32 (2003) 471–476.
[47] C.R. Cho, J.P. Kim, J.Y. Hwang, S.Y. Jeong, Y.G. Joh, D.H. Kim, Jpn. J. Appl. Phys. 43 (2004) L1323–L1326.
[48] T. Tachikawa, T. Majima, Langmuir 25 (2009) 7791–7802.